Electronic Supplementary Material (ESI) for Materials Chemistry Frontiers.

Raman Spectroscopy and Carrier Scattering in 2D Tungsten Disulfides with Vanadium Doping

Jingyun Zou,[a,b*] Yingjie Xu,[a] Xinyue Miao,[a] Hongyu Chen,[a] Rongjie Zhang,[b] Junyang Tan,[b] Lei Tang,[b] Zhengyang Cai,[b] Cheng Zhang,[a] Lixing Kang,[c] Xiaohua Zhang,[d] Chunlan Ma,[a*] Hui-Ming Cheng,[b] and Bilu Liu[b*]

[a] Jiangsu Key Laboratory of Micro and Nano Heat Fluid Flow Technology and Energy Application, School of Physical Science and Technology, Suzhou University of Science and Technology, Suzhou 215009, China

[b] Shenzhen Geim Graphene Center, Tsinghua-Berkeley Shenzhen Institute & Institute of Materials Research, Tsinghua Shenzhen International Graduate School, Tsinghua University, Shenzhen 518055, China

[c] Division of Advanced Nano-Materials, Suzhou Institute of Nano-Tech and Nano-Bionics, Chinese Academy of Sciences, Suzhou, China

[d] Innovation Center for Textile Science and Technology, Donghua University, Shanghai 201620, China

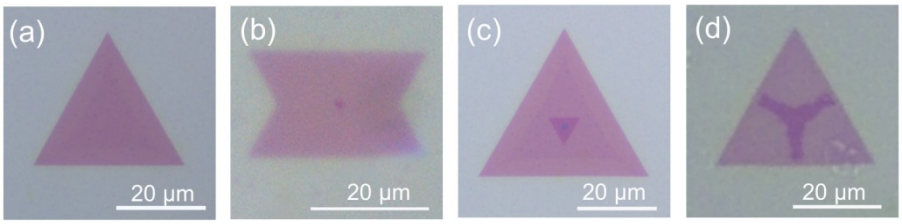

Figure S1. Optical microscope images of the as-grown V-WS_2 flakes with different morphologies. (a) A triangle monolayer, (b) a twinned monolayer V-WS_2, (c) a triangle bilayer, and (d) a windmill-like bilayer flake, respectively. We find that V-WS_2 flakes with different morphologies and layer numbers can be grown by varying the growth parameters, including temperature and additive amount of the V precursors.

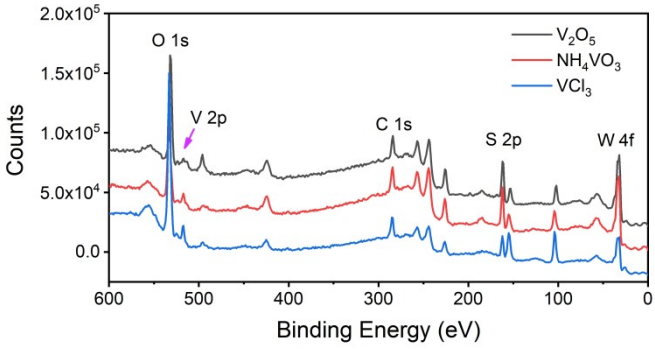

Figure S2. Survey XPS spectra of V-WS_2 flakes doped with V_2O_5, NH_4VO_3, and VCl_3, respectively.

Table S1. Atomic concentration obtained from the XPS characterization in the V-WS_2 flakes

Dopants	W	S	V
V_2O_5	32.3 at%	65.5 at%	2.2 at%
NH_4VO_3	31.1 at%	62.9 at%	6.0 at%
VCl_3	29.3 at%	59.6 at%	11.1 at%

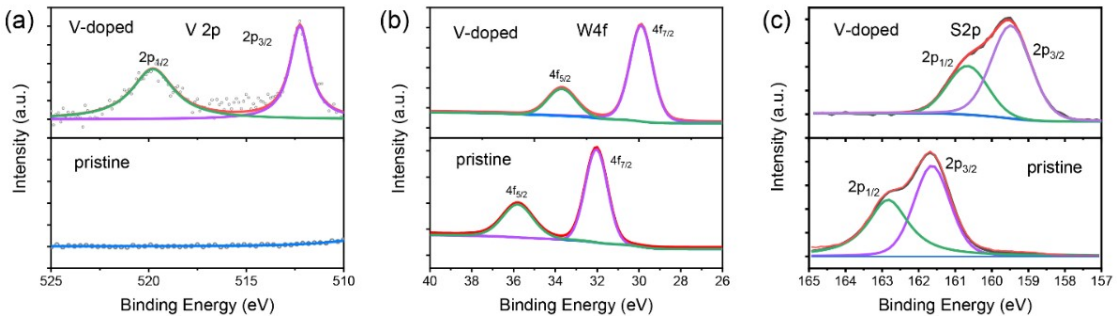

Figure S3. XPS analysis of V-WS_2 doped by VCl_3. (a-c) XPS spectra of the V 2p, W 4f, and S 2p orbitals, respectively. XPS signal of vanadium is observed, confirming the existence of substituted V atoms in the V-WS_2 flake. Meanwhile, both the XPS peaks of W 4f and S 2p orbitals shift toward the low binding energy direction, showing the strong *p*-type doping effect.

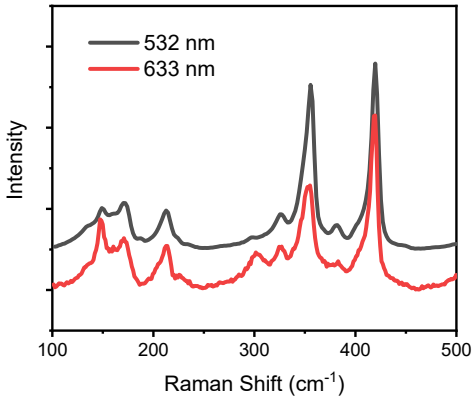

Figure S4. Raman spectra of the V-WS_2 excited by the 532-nm and 633-nm lasers. The two spectra were normalized according to the $A_1'(\Gamma)$ peak. Obviously, though the intensity of $E'(\Gamma)$ and $ZA(M)$ peaks varies with the changed excitation lasers, both the peak position and intensity of P_c nearly do not change, revealing that this Raman peak has no dependence with the wavelength of the excitation lasers.

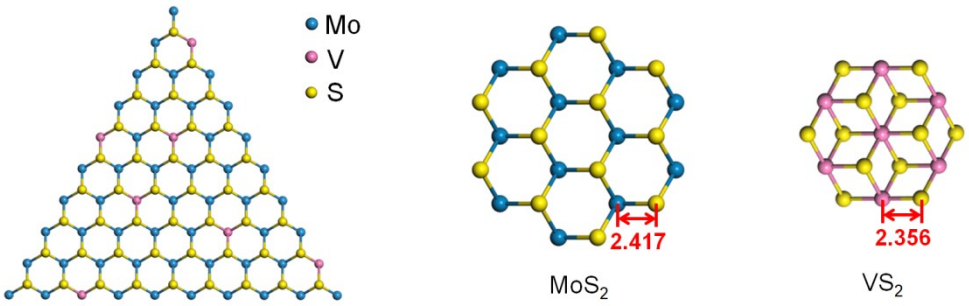

Figure S5. Schematics of the atomic crystal structure of (a) V-doped WS_2, (b) WS_2, and (c) VS_2. The substituted vanadium atoms are uniformly distributed throughout the whole flake. The bond length of VS_2 is 2.356 Å, small than that of MoS_2 (2.417 Å). So, the substituted V atoms will stretch the surrounding Mo-S bonds. A tensile strain is generated in the V-WS_2, which causes the shift of the Raman E_{2g} peak to the low wavenumber direction.

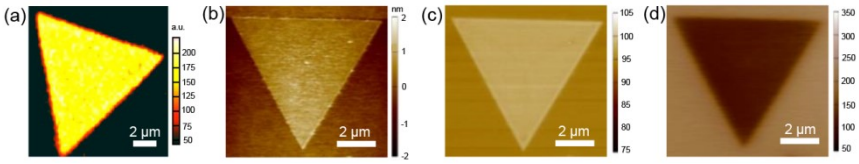

Figure S6. (a) Raman mapping image acquired at 214 cm^{-1}, in which the uniform color profile demonstrates the uniform doping effect. (b) AFM topography image of a monolayer V-WS_2 flake doped with NH_4VO_3 taken at room temperature, and the corresponding (c) EFM and (d) SKPM images.

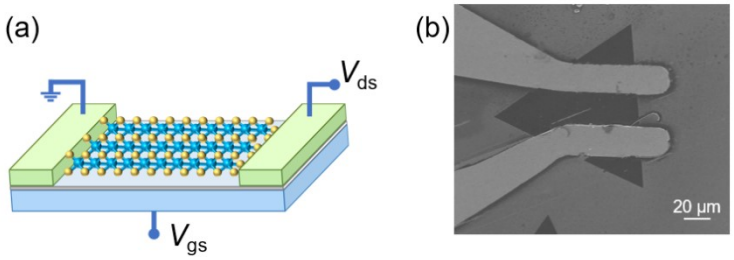

Figure S7. (a) Schematic and (b) SEM image of the back-gated FET with a monolayer V-WS_2 flake as the channel material. The width (*W*) and length (*L*) of the channel are 11.6 μm and 36.9 μm, respectively, yielding an *L*/*W* ratio of 3.18.